Available online at www.sciencedirect.com
SciVerse ScienceDirect
Scripta Materialia 66 (2012) 343–346
Scripta MATERIALIA
www.elsevier.com/locate/scriptamat

Dislocation density measurement by electron channeling contrast imaging in a scanning electron microscope

I. Gutierrez-Urrutia* and D. Raabe

Max-Planck-Institut für Eisenforschung, Max-Planck Str. 1, D-40237 Düsseldorf, Germany

Received 12 October 2011; revised 18 November 2011; accepted 19 November 2011
Available online 30 November 2011

We have measured the average dislocation density by electron channeling contrast imaging (ECCI) in a scanning electron microscope under controlled diffraction conditions in a Fe–3 wt.% Si alloy tensile deformed to a macroscopic stress of 500 MPa. Under optimal diffraction conditions, ECCI provides an average dislocation density close to that obtained by bright-field transmission electron microscopy. This result confirms that ECCI is a powerful technique for determining dislocation densities in deformed bulk metals.
© 2011 Acta Materialia Inc. Published by Elsevier Ltd. All rights reserved.

Keywords: Dislocations; Low-temperature deformation; Electron diffraction; Scanning electron microscopy (SEM); Ferritic steels

The storage of dislocations during deformation of metals plays a key role in most metallurgical phenomena such as strain hardening, damage, creep, fatigue, athermal phase transformations, recrystallization and strain-induced grain boundary migration. In the former cases, it determines the mechanical properties such as strength and ductility. In the latter cases, it plays an important role in the mechanisms acting during annealing and transformation of deformed microstructures. In many cases, the average dislocation density is even linearly related to characteristic phenomena such as strengthening, creep rate, recovery and primary recrystallization. For this reason, the determination of the average dislocation density is important to better understand such phenomena. Dislocation density is commonly measured by direct methods such as transmission electron microscopy (TEM) [1–3] and indirect methods such as X-ray diffraction (XRD) [4,5]. TEM provides a highly accurate determination of the dislocation density provided that the dislocations can be clearly distinguished, i.e. it can be applied with high accuracy below a certain dislocation density ($\sim$5–10 $\times$ 10^{-14} m^{-2}). However, the determination of average dislocation density values in heterogeneous microstructures by TEM is time consuming owing to the demanding sample preparation technique involved. On the other hand, XRD provides an average dislocation density of the bulk deformed material in a shorter time but with a limited spatial resolution. In addition, XRD analysis of defect structures requires the use of a well-justified underlying model that connects a certain dislocation density and distribution with a total displacement gradient field.

An alternative microscopy technique for characterizing deformed microstructures is electron channeling contrast imaging (ECCI) [6–9]. ECCI is a scanning electron microscopy (SEM) technique that makes use of the fact that the backscattered electron intensity is strongly dependent on the orientation of the crystal lattice planes with respect to the incident electron beam due to the electron channeling mechanism. Slight local distortions in the crystal lattice due to dislocations cause a modulation of the backscattered electron intensity, allowing the defect to be imaged. The ECCI technique has been used to image dislocation structures in metals deformed during fatigue loading [10] or in the vicinity of cracks [11], and even stacking faults [12]. In particular, we have recently characterized complex mixed dislocation and twin substructures, as well as their individual contributions to strain hardening, on a highly deformed Fe–22 wt.% Mn–0.6 wt.% C alloy [13,14] by ECCI. For this purpose we used a novel ECCI set-up [9] which makes use of combined electron backscatter diffraction (EBSD) to image dislocations at enhanced contrast. In this paper, we demonstrate that the ECCI technique allows the determination of the average dislocation density of a deformed metal. The aim of the work is to establish ECCI

* Corresponding author. Tel.: +49 2116792 407; e-mail: i.gutierrez@mpie.de

1359-6462/$ - see front matter © 2011 Acta Materialia Inc. Published by Elsevier Ltd. All rights reserved.
doi:10.1016/j.scriptamat.2011.11.027

as a very powerful, versatile, fast and experimentally robust method for determining dislocation defects densities and arrangements that involves a relatively simple preparation process. For this reason we used ECCI to measure the average dislocation density in a Fe–3 wt.% Si alloy tensile deformed to a macroscopic stress of 500 MPa. Under optimal diffraction conditions, the ECCI technique provides an average dislocation density close to that obtained by bright-field TEM.

The material selected was a Fe–3 wt.% Si alloy sheet 260 μm thick supplied by ThyssenKrupp Electrical Steel GmbH. The material has a large grain size in the centimeter range and a strong Goss texture {1 1 0}<0 0 1>. This microstructure makes the sample suited for the measurement of the dislocation density. Tensile tests were performed at room temperature at a strain rate of $2 \times 10^{-3}\,s^{-1}$ to a macroscopic stress of 500 MPa. The mechanical tests were carried out using test instrument of Kammrath & Weiss GmbH (44141 Dortmund, Germany) equipped with a digital image correlation (DIC) system (ARAMIS system, GOM-Gesellschaft für Optische Messtechnik mbH, 38106 Braunschweig, Germany) for measuring the local strain. Details of this set-up are described in Ref. [15]. The surface pattern required for DIC was obtained as explained in Ref. [13]. Dislocation densities were measured in areas with a local strain of 0.05 by means of ECCI. A new recently reported set-up for ECCI [9] was used in this study to obtain ECCI images under controlled diffraction conditions which produced an enhanced dislocation contrast. This ECCI set-up has been successfully used in the imaging of dislocation substructures in Fe-based alloys [13,14]. The set-up uses EBSD patterns for calculating the optimal orientation of the crystal inspected through a specific combination of tilts and rotations. These are determined from the corresponding calculated diffraction pattern using the algorithm developed in Ref. [16]. ECCI observations were carried out in a Zeiss Crossbeam instrument (XB 1540, Carl Zeiss SMT AG, Germany) consisting of a Gemini-type field emission gun (FEG) electron column and a focused ion beam (FIB) device (Orsay Physics). ECCI was performed at 10 kV acceleration voltage and a working distance of 6 mm, using a solid-state four-quadrant backscattered electron detector. ECCI images were obtained with the sample normal aligned parallel to the incident electron beam.

It is well known that optimum dislocation contrast in ECCI is obtained by orienting the crystal to the exact Bragg angle, i.e. $s = 0$ where s is the deviation vector, in a two-beam condition [8,17]. Dislocation contrast becomes weaker under diffraction conditions deviating from the optimal, i.e. when $s \neq 0$. However, the latter, although not optimal, can be useful in the determination of the average dislocation density, as we show below. In the present work, we have evaluated the influence of diffraction condition in the determination of the average dislocation density. Dislocation densities were determined from ECC images that were taken under two different diffraction conditions, namely two-beam conditions with one set of *hkl* planes at the Bragg angle, and, alternatively, three-beam cases with two sets of *hkl* planes in an out-of-Bragg condition. For the first diffraction condition, dislocations appear as sharp bright lines over a dark background, whereas in the second diffraction condition, dislocations are visible as bright and dark sharp lines over a brighter background.

Figure 1 shows examples of ECC images of dislocation arrangements at the same area under different diffraction conditions with the corresponding calculated diffraction patterns. The ECC image of Figure 1a was obtained after orienting the crystal into Bragg condition using a high-intensity reflection of (1 1 0)-type. The calculated diffraction pattern is shown in Figure 1b. Under this diffraction condition, the crystal matrix appears dark and dislocations appear as sharp bright lines. The ECC image presented in Figure 1c was obtained after orienting the crystal out of the Bragg condition with $s < 0$. The calculated diffraction pattern is shown in Figure 1d. In this orientation, the crystal matrix appears brighter than in Bragg condition due to electron channeling mechanism [8]. In the first case, electrons are more effectively channeled into the lattice and the backscattering yield is low, leading to a dark appearance of the crystal. In the second case, the backscattering yield is enhanced and the crystal appears bright. In Figure 1c, we can identify dislocations appearing as white and black lines with uniform and sharp contrast. According to the dislocation contrast theory developed for TEM, the dislocation contrast exhibits an oscillatory black–white color with a periodicity of ξ_g, where ξ_g is the extinction distance [3]. Spencer et al. [17] showed that in ECCI, similar to TEM, the oscillatory behavior disappears for a dislocation that is located deeper than $2\xi_g$ from the sample surface, due to anomalous absorption phenomena related with inelastic scattering processes. According to the dislocation contrast profiles calculated by the authors [11], in a two-beam condition with one set of *hkl* planes at or close to Bragg orientation, dislocations exhibit a uniform white contrast. As in ECCI the $g.b = 0$ invisibility criterion holds [8,18,19], we can ascribe the bright sharp dislocations to those fulfilling $g.b \neq 0$ with g: 110, where b is the Burgers vector and g the diffraction vector. The origin of the

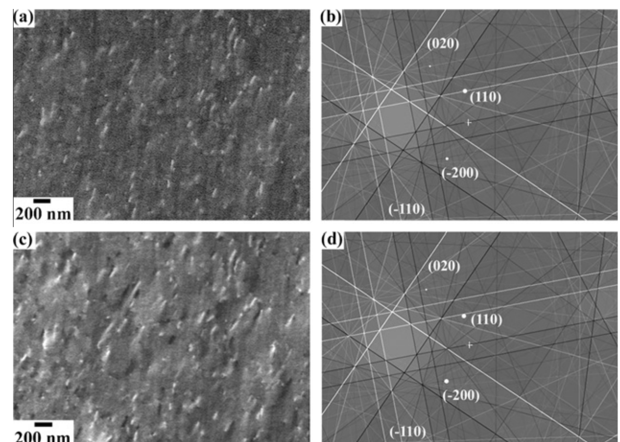

Figure 1. ECC images of dislocation arrangements of the same area in a Fe–3 wt.% Si alloy tensile deformed to a macroscopic stress of 500 MPa under two different diffraction conditions with the corresponding calculated diffraction pattern: (a and b) two-beam condition with g: 110 at Bragg orientation; (c and d) three-beam condition with g: 110 and g: −200 out-of-Bragg (g is the diffraction vector).

sharp black dislocation contrast observed in Figure 1c can be attributed to the deviation from the two-beam condition. As the calculated diffraction pattern of Figure 1d reveals, the (−2 0 0) reflector, which is out of Bragg condition with $s << 0$, is excited as well, although it is less strong than g: 110, i.e. it corresponds to a three-beam condition. Accordingly, these dislocations fulfill $g.b \neq 0$ with g: −2 0 0 and, due to $s << 0$, exhibit a black contrast. In fact, this is the origin of the diffuse black dislocation contrast in the ECC image revealed in Figure 1a, as the calculated diffraction pattern of Figure 1b shows. Under the present microscope conditions with an acceleration voltage of 10 kV, anomalous absorption occurs at depths higher than about $2\xi_{200} \approx 26$ nm for the diffraction conditions used here. As most of the visible dislocations exhibit a uniform contrast, this indicates that dislocations visible by ECCI in the present study are placed deeper than 26 nm from the sample surface.

Average dislocation densities, ρ, were estimated using the relationship: $\rho = 2\ N/Lt$, where N is the number of dislocation lines intersecting a grid of total line length L on the corresponding ECC image and t is the probe depth. This is a standard relationship used in TEM when the individual dislocations can be clearly distinguished, like in the present study [1,20]. Dislocations were measured from ECC images similar to those shown in Figure 1. As example, Figure 2 depicts a drawing of the dislocations (black lines) imaged under the diffraction conditions of Figure 1a and c. Dislocations are identified according to the dislocation contrast of the corresponding diffraction condition, namely bright lines in Figure 1a and bright and dark lines in Figure 1c. Only dislocations with a well-defined and sharp contrast are considered. Figure 1c reveals that some dislocations with black contrast exhibit a blurred contrast, which is mainly ascribed to the multi-beam diffraction condition with $s < 0$. However, these dislocations can also be clearly identified. It can be seen that the number of dislocations identified in Figure 2b is higher than in Figure 2a. This is ascribed to the higher number of excited reflectors which provides two types of dislocation contrast, i.e. black and white. The probe depth for imaging dislocations in ECCI is a difficult parameter to calculate due to the complexity of modeling the backscattering of electrons from a thick crystalline material. However, Wilkinson et al. [7] have calculated ECC image profiles of dislocations based on the theoretical approach of channeling contrast formation suggested by Spencer et al. [17], and estimated the limiting probe depth for imaging dislocations in ECCI, which is about $5\xi_g$. Assuming this probe depth and under the present ECCI conditions (acceleration voltage of 10 kV, and corresponding values of ξ_g for Fe [21]), the probe depth ranges from 45 to 65 nm for the diffraction vectors g used in the present study ((1 1 0) and (2 0 0)-type). The estimated average dislocation densities are plotted in Figure 3. Under three-beam conditions, the largest probe depth was used. Average dislocation densities of $10 \pm 4 \times 10^{-13}$ and $17 \pm 6 \times 10^{-13}\ \mathrm{m}^{-2}$ were obtained from the ECC images under two-beam conditions with one set of *hkl* planes at Bragg orientation and three-beam conditions with two sets of *hkl* planes out-of-Bragg, respectively. We should emphasize here that the multi-beam conditions used to estimate the average dislocation density are similar to those shown in Figure 1c and d. As Figure 1 reveals, the higher average density obtained by the second diffraction condition is ascribed to the higher number of excited reflectors, which provides, due to channeling mechanism, a higher amount of visible dislocations.

To compare the present estimations of the average dislocation density measured by ECCI to that determined by a standard characterization technique such as TEM, we have included in Figure 3 the average dislocation density measured in a Fe–3 wt.% Si sample deformed to the same macroscopic stress level (500 MPa) by bright-field TEM. The average dislocation density was measured from TEM micrographs using the same method as in the present work [22]. It can be seen that the average dislocation density estimated from ECCI is in the same range than that determined from bright-field

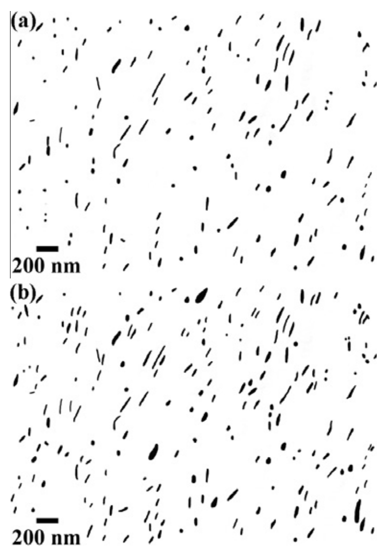

Figure 2. Schematic drawings of the dislocations (black lines) imaged by ECCI as shown in Figure 1: (a) corresponds to Figure 1a, (b) corresponds to Figure 1c. See the text for details of the identification procedure.

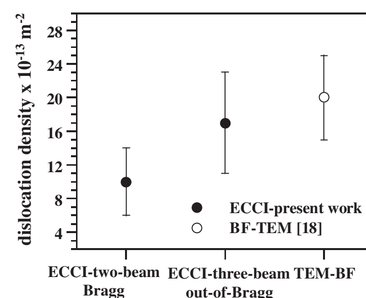

Figure 3. Average dislocation densities determined in a Fe–3 wt.% Si alloy tensile deformed to a macroscopic stress of 500 MPa by two different electron microscopy techniques: ECCI and TEM. Average dislocation densities were measured by ECCI under two different diffraction conditions: two-beam conditions with one set of *hkl* planes in the Bragg orientation (Fig. 1a and b) and three-beam diffraction conditions with two sets of *hkl* planes out-of-Bragg (Fig. 1c and d) (BF: bright field).

TEM. In particular, the average dislocation density measured by ECCI in two-beam conditions with one set of *hkl* planes at the Bragg orientation represents a lower-bound value for the dislocation density. This result is well-known from corresponding TEM-based estimates [1]. The present work shows that three-beam diffraction conditions with two sets of *hkl* planes out-of-Bragg provide a better estimation of the average dislocation density by ECCI, close to that obtained by bright-field TEM. Further, this study confirms ECCI as a powerful technique to determine dislocation densities in deformed bulk metals at a wide field of view. This is a significant advance in microstructural characterization of deformed materials where dislocation densities are typically determined by TEM or XRD. As ECCI is a SEM-based technique it has the advantage over TEM that much larger areas can be observed and samples are easier to prepare. However, due to the small size of the features imaged in this study, namely dislocation lines, the determination of dislocation densities is here performed on areas comparable to those used in TEM. Furthermore, in TEM, the wedge-shape geometry of the foil also makes it necessary to measure the sample thickness in each analyzed material portion. In ECCI, the probe depth only depends on the acceleration voltage and diffraction vector through the extinction distance. In particular, in an oxide-free surface and operating at constant acceleration voltage, the probe depth is only determined by the diffraction vector. It is worth mentioning that in the present ECCI–EBSD approach dislocations are imaged in the scanning electron microscope directly from the collected electron backscattered signal. Accordingly, the estimated dislocation density comprises both types of dislocations, namely geometrically necessary dislocations (GND) and statistically stored dislocations (SSD). Recently, there is an increasing interest in the determination of the GND density via EBSD-based approaches. These methods are based on the measurement of orientation gradients by electron backscatter diffraction patterns and the subsequent dislocation density tensor calculation [23–25]. Considering the current experimental limitations in the determination of orientation gradients via EBSD [26], these methods can provide microstructurally based insights into the mechanisms of strain hardening and size-dependent plasticity. However, the calculated dislocation density is a lower bound of the total dislocation density because only GNDs are considered. In this regard, the present ECCI–EBSD approach provides a better estimate of the total dislocation density, which is similar to that obtained by conventional TEM, as confirmed by the present results.

In summary, the average dislocation density in a Fe–3 wt.% Si alloy tensile deformed to a macroscopic stress of 500 MPa has been determined by ECCI using a novel SEM-EBSD-based set-up. We have studied the influence of the diffraction conditions on the measurement of the dislocation density in ECCI. Under optimum diffraction conditions, ECCI provides an average dislocation density close to that obtained by standard bright-field TEM. This result confirms that ECCI is a powerful and versatile wide-field-of-view technique to determine dislocation densities in deformed metals.

The authors would like to acknowledge the financial support by the German Research Foundation in the framework of the SFB 761 “steel ab initio”.

[1] P. Hirsch, A. Howie, R.B. Nicholson, D.W. Pashley, M.J. Whelan, Electron Microscopy of Thin Crystals, Robert E. Krieger, Huntington, NY, 1977.
[2] G. Thomas, M.J. Goringe, Transmission Electron Microscopy of Materials, John Wiley & Sons, New York, 1979.
[3] D.B. Williams, C.B. Carter, Transmission Electron Microscopy. A Textbook for Materials Science, Springer Verlag, Berlin, 2009.
[4] T. Ungár, H. Mughrabi, M. Wilkens, Acta Metall. 30 (1982) 1861.
[5] T. Ungár, S. Ott, P.G. Sanders, A. Borbély, J.R. Weertman, Acta Mater. 46 (1998) 3693.
[6] D.C. Joy, D.E. Newbury, D.L. Davidson, Rev. Phys. Appl. 53 (1982) 81.
[7] A.J. Wilkinson, G.R. Anstis, J.T. Czernuszka, N.J. Long, P.B. Hirsch, Philos. Mag. A 68 (1993) 59.
[8] A.J. Wilkinson, P.B. Hirsch, Micron 28 (1997) 279.
[9] I. Gutierrez-Urrutia, S. Zaefferer, D. Raabe, Scr. Mater. 61 (2009) 737.
[10] Z.F. Zhang, Z.G. Wang, Z.M. Sun, Acta Mater. 49 (2001) 2875.
[11] B.C. Ng, B.A. Simkin, M.A. Crimp, Ultramicroscopy 75 (1998) 137.
[12] A. Weidner, S. Martin, V. Klemm, U. Martin, H. Biermann, Scr. Mater. 64 (2011) 513.
[13] I. Gutierrez-Urrutia, S. Zaefferer, D. Raabe, Mater. Sci. Eng. A 527 (2010) 3552.
[14] I. Gutierrez-Urrutia, D. Raabe, Acta Mater. 59 (2011) 6449.
[15] D. Raabe, M. Sachtleber, Z. Zhao, F. Roters, S. Zaefferer, Acta Mater. 49 (2001) 3433.
[16] S. Zaefferer, J. Appl. Crystallogr. 33 (2000) 10.
[17] J.P. Spencer, C.J. Humphreys, P.B. Hirsch, Philos. Mag. 26 (1972) 193.
[18] A.J. Wilkinson, P.B. Hirsch, Philos. Mag. A 72 (1995) 81.
[19] M.A. Crimp, B.A. Simkin, B.C. Ng, Philos. Mag. Lett. 81 (2001) 833.
[20] R.K. Ham, Philos. Mag. 69 (1961) 1183.
[21] L. Reimer, H. Kohl, Transmission Electron Microscopy. Physics of Image Formation, Springer Verlag, Berlin, 2008.
[22] D. Griffiths, J.N. Riley, Acta Metall. 14 (1966) 755.
[23] E. Demir, D. Raabe, N. Zaafarani, S. Zaefferer, Acta Mater. 57 (2009) 559.
[24] S. Sun, B.L. Adams, W.E. King, Philos. Mag. A 80 (2000) 9.
[25] L.P. Kubin, A. Mortensen, Scr. Mater. 48 (2003) 119.
[26] T.B. Britton, C. Maurice, R. Fortunier, J.H. Driver, A.P. Day, G. Meaden, D.J. Dingley, K. Mingard, A.J. Wilkinson, Ultramicroscopy 110 (2010) 1443.